ick here to download LaTeX File (.tex, .sty, .cls, .bst, .bib): article.tex
Generated using version 3.1.1 of the official AMS LaTeX template

CheapAML: A simple, atmospheric boundary layer model for use in ocean-only model calculations

BRUNO DEREMBLE * N. WIENDERS AND W.K. DEWAR

Department of Earth, Ocean and Atmospheric Science,

Florida State University, Tallahassee, Florida

* *Corresponding author address:* Bruno Deremble, Florida State University, 117 N. Woodward Ave., Tallahassee, FL 32306-4320

E-mail: bderemble@fsu.edu

ABSTRACT

We develop a model of the marine atmospheric boundary layer for ocean-only modeling in order to better represent air-sea exchanges. This model computes the evolution of the atmospheric boundary layer temperature and humidity using a prescribed wind field. These quantities react to the underlying ocean through turbulent and radiative fluxes. With two examples, we illustrate that this formulation is accurate for regional and global modeling purposes and that turbulent fluxes are well reproduced in test cases when compared to reanalysis products. The model builds upon and is an extension of Seager et al. (1995).

1. Introduction

The ocean surface exerts strong control on the atmospheric boundary layer through momentum, heat and moisture exchange across the ocean-atmosphere interface. Realistic ocean modeling places a premium on this influence, but common practices can omit it. For example, specifying fluxes at the ocean surface misses this connection; thereby, for example, locating strong oceanic heat loss away from the subsurface structure they should be associated with. Even high resolution, high accuracy scatterometer wind stress data can be uncorrelated with the surface velocity expression of a free running ocean simulation. Another common approach consists of specifying atmospheric temperature, humidity and wind and then diagnosing from them air-sea fluxes with a bulk equation. However, the ocean naturally develops scales much finer than the resolutions currently available from all atmospheric reanalysis products, and the imprint of these scales on the exchanges, with any subsequent feedbacks on the atmospheric variables, are lost. Given the low heat capacity of the atmosphere, the reaction of the atmosphere can be strong, thus influencing later heat exchanges and precipitation.

To fully capture the ocean-atmosphere connection at the interface would require a fully coupled ocean-atmosphere model. It is an open question if such a thing currently exists, however, even if it did, the computational burden associated with its use would be restrictive. It is thus of practical value to have alternatives that replicate at least some of the important coupling features.

Seager et al. (1995; S95 hereafter) in an insightful paper, recommended a partial solution to this problem. They proposed the use of a thermodynamically active, but dynamically passive, atmospheric boundary layer. The wind was specified, relieving the need to compute atmospheric dynamics, and with an assumption of rapid equilibration of the atmospheric temperature and humidity, the atmospheric state was diagnosed. Applications in models showed clear improvement in the flux structure relative to other products. Such an approach provides a means of overcoming many of the leading order omissions in ocean modeling associated with either flux specification, the use of bulk formulae or relaxation boundary conditions while simultaneously retaining the computational efficiency and flexibility inherent in ocean only modeling.

Our goal here is to modernize the S95 thermodynamic atmospheric boundary layer model. The four primary distinctions between our approach and that of S95 are in the (1) use of modern flux algorithms, (2) abandonment of the equilibrium assumption, (3) calculation of an accurate fresh water flux and (4) ease of migration to parallel computing. Specifically, the modular model design permits the user to either develop a subroutine using the flux algorithms of their choice, or to choose from the methods of Large and Pond (1982); hereafter LP82 or COARE3 (Fairall et al. 2003). We discard the equilibrium assumption because modern computing involves specifying atmospheric data typically at rates of a few times per day, as opposed to the use of lower frequency climatological data as was the custom at the time of S95's original paper. Coupled with this is the prediction, rather than diagnosis, of the atmospheric state, which removes the need to solve an elliptic equation. The latter, aside from suppressing 'weather' responses, are difficult to efficiently migrate to parallel platforms. The impact of the equilibrium hypothesis has been studied by Hazeleger et al. (2001). They added a parameterization of atmospheric storms to S95 and found significant impacts in several regions of the Pacific. The use of daily wind (as opposed to a monthly climatology) greatly modifies latent and sensible heat fluxes as well. Indeed the sensible heat fluxes scales as $\propto u\Delta T$, with u the magnitude of the surface wind and ΔT the temperature difference between the ocean and the atmosphere. When suppressing the variability of u and ΔT by taking a mean value, it appears that the fluxes will be systematically underestimated, especially when the variability of u is large (not shown).

Our model, named CheapAML, has been implemented in the MIT General Circulation Model (MITgcm) and is available with the standard distribution as a package. This fortran code computes the forced atmospheric temperature and relative humidity tendency terms; it can be downloaded and modified for any model.

In principle, this atmospheric module can be applied to any model configuration, e.g. coarse grids, eddy resolutions and for regional to global configurations, without tuning. However, we show in the following that in certain regions, this model can introduce a drift due to unmodelled physical processes. In such regions (mainly the tropics), it is preferable to adjust some parameters or to introduce a relaxation towards climatological values. Another limitation might be the availability of a fine resolution wind field (spatial and temporal) for meso- or submeso-scale ocean applications. We discuss the effect of wind-SST interaction (Small et al. (2008)) even though this has not been implemented in CheapAML.

The paper is organized as follows. The model is described in Section 2. In Sections 3 and 4 we describe the results of two verification experiments. First a regional experiment in the Gulf Stream is presented, followed by a global modeling application. The conclusions are given in Section 5. Appendix A compares several methods currently available to compute latent and sensible heat flux.

2. Model Equations

a. Main equations

The basic assumptions of CheapAML are that atmospheric reanalysis variables like humidity and temperature are accurate on large scales and of these the least sensitive to ocean surface structure is velocity. We thus accept atmospheric velocity as a known and develop equations governing the atmospheric tracer fields of temperature and water. This shortcut avoids the complexities of atmospheric dynamics and instead concentrates on thermodynamics. The shortcomings of this assumption are discussed by Small et al. (2008) who demonstrate that the wind can be modified by ocean mesoscale eddies. This in turn can impact air-sea fluxes. Including this in our boundary layer model would essentially turn it into a coupled model and we opt not to do so. The fundamental equation solved by CheapAML is:

$$s_t + ADV(s) = -F_z + \nabla \cdot (K \nabla s) - \lambda(s - s_c)\,, \tag{1}$$

where s is either atmospheric potential temperature, T (degrees Celsius), or water vapor content, q (kg water/kg air), F is the appropriate property flux whose vertical divergence influences s, K is an atmospheric diffusivity, λ is an inverse of a relaxation time scale, and s_c is a specified value of temperature or humidity. We later discuss the impact of this relaxation term. The advection term is written in Boussinesq divergence form as

$$ADV(s) = \nabla \cdot (\boldsymbol{u} s)\,. \tag{2}$$

Most atmospheric reanalysis products provide horizontal wind velocities at a given height (10 m often). These are used in the solution of (1), and for this reason, we regard (1) as representing the evolution of the tracer s at the standard height. Some advection schemes, like many monotone methods, require a three-dimensional velocity field, and later on we will argue that the calculation of precipitation is improved when including the vertical velocity as part of the computation. Consequently, vertical velocity, w, is diagnosed according to

$$w_z = -(u_x + v_y)\,. \tag{3}$$

We also employ the simplifying assumption that the atmospheric boundary layer is described by a known, but possibly variable, thickness h. The model also employs a specification of the tracers s over land and allows time dependence in those specifications.

The tracers are governed by the forced advection and diffusion equation (1). The physical forcing is assumed to be governed primarily by turbulent vertical transports whose divergence enters into tracer evolution. For potential temperature, the vertical flux divergence at the standard height is estimated using

$$-F_z^T = \frac{F^+ - F^-}{\rho_a C_p h}\,, \tag{4}$$

where h is the boundary layer thickness, ρ_a the atmospheric density, C_p the atmospheric heat capacity and $F^{+,-}$ represents the energy fluxes at the top and bottom of the layer, respectively. Employing the convention that positive fluxes are upward, the formulae for the fluxes are

$$F^+ = -F_s^{\downarrow} + \frac{F_l^{\uparrow}}{2} + L\,, \tag{5}$$

$$F^- = -F_s^{\downarrow} + \frac{F_l^{\downarrow}}{2} + F_{ol}^{\uparrow} + L + S\,, \tag{6}$$

where $F_s^{\downarrow}$ is the solar short wave flux, $F_l^{\uparrow\downarrow}$ the up and downwelled atmospheric long wave flux, $F_{ol}^{\uparrow}$ the upwelled oceanic long wave flux, L latent heat flux and S sensible heat flux. The boundary layer model is meant as a sub cloud layer model, implying that condensation happens at the top of the boundary layer. Therefore the latent heat release associated with the condensation is not realized in the boundary layer, but instead escapes to the atmosphere above. The latent flux, L, is thus common to both the formulae in Eqs. (5-6). These turbulent fluxes are computed using a user chosen algorithm (currently, the options are LP82 or COARE3 algorithms).

Note that solar shortwave is common to both fluxes, implying that it transits the atmospheric layer without loss. This is not precisely true, but implies that the contents of solar forcing should be the net forcing absorbed at the surface, accounting for albedo reflection. Long wave radiation is computed according to the standard Stefan-Boltzmann law:

$$F_l = \epsilon\sigma T^4\,, \tag{7}$$

where ϵ is an emissivity. These empirical parameterizations have been found to yield accurate estimates and are consistent with approximations about the optical depths of the atmosphere reflecting the level of model simplification (Talley et al. 2011).

In order to accurately compute the net heat flux at the ocean surface, we must account for the emission of long wave radiations by clouds and aerosols. The dynamics are not simple and depend upon detailed cloud structure. Clark et al. (1974) proposed a formulation for the net longwave at the ocean surface (see also the review by Josey et al. 1997):

$$F_l^{net} = \epsilon\sigma SST^4(0.39 - 0.05\sqrt{e})(1 - \lambda C^2) + 4\epsilon\sigma SST^3(SST - T)\,, \tag{8}$$

with C an externally provided cloud fraction, e the water pressure in millibar and λ is a latitude dependent coefficient. We use here $\lambda = 0.5 + |latitude|/230$ (see Clark et al. 1974), and the latitude expressed in degrees from the equator.

Water vapor forcing takes the form:

$$-F_z^q = \frac{E - F_q^{\uparrow}}{\rho_a h}, \tag{9}$$

where E and $F_q^{\uparrow}$ represent evaporation and moisture entrainment at the top of the boundary layer respectively. Evaporation is computed as the latent heat flux divided by the latent heat of evaporation.

The flux of humidity $F_q^{\uparrow}$ at the top of the boundary layer parameterizes water vapor entrainment and transport at the top of the boundary layer. We retain the same parameterization as S95:

$$F_q^{\uparrow} = \mu\rho_a C_{de}|\boldsymbol{u}|q\,, \tag{10}$$

with C_{de} the exchange coefficient for evaporation, $|\boldsymbol{u}|$ the magnitude of the wind (see Sec. 2b), and μ a coefficient set to 0.25 (see also the discussion in S95). If we interpret the coefficient in Eq. (10) as a entrainment time scale τ_e, we have

$$\tau_e \sim \frac{h}{\mu C_{de}|\boldsymbol{u}|} \simeq 10 \text{ days}\,, \tag{11}$$

using the approximation $C_{de} = 10^{-3}$ and $|\boldsymbol{u}| = 5$ m s^{-1}. These numbers may vary but do provide a time scale of the entrainment at the top of the boundary layer.

Precipitation is generally one of the most difficult atmospheric variables to predict and a model of this simplicity will suffer when applied to the wide variety of realistic precipitative conditions. Precipitation in the boundary layer only enters the water vapor budget as a small correction and we chose to not retain it. We only compute it as a diagnostic field for the ocean fresh water budget.

We here describe a parameterization that is physically justified and which has performed reasonably well in tests. The applications in the next sections illustrate its strengths and weaknesses, and we provide methods by which the weaknesses can be addressed.

In our parameterization, precipitation is directly related to vertical wind. We allow precipitation only if the vertical wind, w, is upward and adjust the precipitation according to the size of w. We compute the large scale precipitation (LSP) as:

$$\mathrm{LSP} = \max(\rho_a h \frac{q - 0.7 q_s}{\tau_1} \left(\frac{w}{w_0}\right)^2, 0)\,, \tag{12}$$

q_s being the saturation specific humidity at the temperature T, τ_1 a precipitation time scale, w the vertical velocity, w_0 a reference vertical velocity. The multiplicative nondimensional term modulates the strength of the precipitation using a threshold set with w_0. The square factor is set to better separate high and low values of vertical wind. The numerical values used in the following examples are: $\tau_1 = 40$ h and $w_0 = 7.5 \times 10^{-6}$ m s^{-1}. The value of τ_1 is not really the precipitation time scale since it is modulated by $(w/w_0)^2$. The pattern of $(w/w_0)^2$ is essentially zero and reaches values of 10 in regions of intense upward wind.

This parameterization systematically underestimates precipitation near the equator. We therefor add a correction for the region where $q > 0.2$ kg/kg (see Fig. 7); the convective precipitation (CP) is computed as

$$\mathrm{CP} = \max(\rho_a h \frac{q - 0.9 q_s}{\tau_2}, 0)\,, \tag{13}$$

with $\tau_2 = 6$ h. All these constants have been determined manually to match predicted and observed patterns. Parameter estimation via regression has proven unreliable since precipitation is a very localized event. We assume that runoff is part of the ocean-land interaction and is thus not represented here.

b. Air-sea turbulent fluxes

Several algorithms computing the turbulent momentum, heat and water fluxes at the air-sea interface have been developed. An early attempt in wide usage is that in LP82, who provide a formula for the primary drag C_d in terms of the air speed. They then proceed to compute evaporation, sensible heat and stress according to

$$E = C_{de}|\boldsymbol{u}|(q_s^{SST} - q)\,, \tag{14a}$$

$$S = C_{dh}|\boldsymbol{u}|(SST - T)\,, \tag{14b}$$

$$\tau = C_{dd}|\boldsymbol{u}|^2\,, \tag{14c}$$

where the coefficients C_{dx} are computed simultaneously and q_s^{SST} is the saturation specific humidity of the atmosphere evaluated at the local sea surface temperature. This flux calculation has recently been revisited by Fairall et al. (2003), who use Monin-Obukov similarity theory to relate observations of atmospheric variables at standard heights and the stability of the air column to air-sea fluxes. Provision is also made for the ocean wave state, when computing the so-called roughness length. Our implementation of the COARE3 algorithm assumes by default the wave model of Smith (1988) dependent upon the wind, but also permits the specification of wave data. Other flux parameterizations are available, such as Beljaars (1994) although they have not been added to CheapAML as of this writing: only LP82 and COARE3 have been implemented. The various parameterizations yield somewhat distinct estimates for the fluxes, as shown in Appendix A.

c. *Boundary values and relaxation*

CheapAML also requires the specification of the tracer s on the lateral boundaries (when implemented in an open boundary configuration) and on land, and allows time dependence in those specifications. The current version of CheapAML does not include a land module. Instead, the temperature and humidity are strongly relaxed toward provided, and possibly time varying, fields. This is the primary role of the last term of Eq. (1); thus, default specifications are $1/\lambda = 2$ hours over land and $\lambda = 0$ over the ocean. A secondary use of the λ parameter is to nudge the model towards observations in the manner of data assimilation and thus correct for missing model physics. The quantity λ can be specified as a field variable to facilitate this, with the limit of large λ everywhere converging to the classical case where atmospheric variables are specified and fluxes are computed using bulk formulae.

d. *Height of the boundary layer*

The vertical fluxes of temperature and humidity given in Eqs. (4) and (9) both depend on the height of the boundary layer h. The default configuration of CheapAML assumes a uniform h value of 1000 m, a value which provides demonstrably useful fluxes. However, our experience is that it is often advantageous to provide CheapAML with readily available boundary layer thickness data. For example, for global configurations, a constant, single value for the boundary layer height fails to return broadly accurate fluxes and marine boundary layer behavior. In the extra tropics, h varies seasonally from lower than 500 m in the summer to more than 1200 m in the winter. In the tropics h remains between 600 m and 1000 m all year long. CheapAML is designed to optionally accept temporally varying h values, such as are available from the ERA reanalysis data set.

In all the following experiments, we use the daily varying climatology of the boundary layer height provided by the ERA data set.

3. A Regional experiment

a. Mean and variability

To illustrate and assess CheapAML performance, we apply our model to the separated Gulf Stream (GS), where ocean eddying, weather and flux are particularly strong. Here, the SST can vary by more than 10 degrees C over 100 km, which is precisely the characteristic grid space of common reanalysis data sets (Kalnay et al. (1996) for the NCEP/NCAR reanalysis, Uppala et al. (2005) for the ERA reanalysis).

We examine here how CheapAML compares to ERA atmospheric temperature, humidity and fluxes in a confined regional configuration with prescribed SST. The boundaries of the chosen domain are 75°W – 45°W in longitude and 34°N – 45°N in latitude. 'Truth' fluxes have been computed by specifying ERA wind velocity, temperature and humidity at six hourly intervals, with linear interpolation to times in between. CheapAML fluxes are computed by specifying boundary atmospheric variables and default λ values. The underlying SST also comes from the ERA data set. Here again, at each time step, the SST is interpolated between the two nearest records. All fields are spatially interpolated to the finer resolution of 1/12 degrees in latitude and 1/10 degree in longitude (a roughly isotropic grid). 'Truth' is accepted as the ERA computed fluxes.

Figures 1 and 2 summarize the evolution of the atmospheric variables for January, 2007. We plot the monthly mean CheapAML and ERA atmospheric temperature and humidity. The mean temperature difference between CheapAML and ERA does not exceed 0.7 degrees C (Fig. 1). There is a cold bias of CheapAML relative to the 'Truth' over the GS path and a warm bias elsewhere. There is also good agreement in the variability pattern of temperature (computed on a daily basis) in both cases. It is slightly over estimated by 0.7 degrees C over the cold side of the GS and underestimated by 0.5 degrees C over the warm side.

We draw similar conclusions when looking at the mean and standard deviation of daily values of humidity (Fig. 2). The mean humidity is overestimated outside of the GS path by 0.8 g/kg in accordance with the temperature bias. The pattern of variability has a similar shape in ERA and CheapAML. In the latter, it is underestimated everywhere with a maximum over the warm side of the front.

The heat and moisture fluxes (not shown) also show similar results, i.e. differences are in the 10–20% range, which is well within the uncertainty of bulk flux parameterizations (see also Appendix A). Comparable results are found if fluxes are computed using the S95 approach. An improvement of CheapAML relative to S95 lies in the variability pattern. The variability of temperature and humidity are underestimated over the entire region by more than 1 degree C and 1 g/kg respectively by S95. This relatively weak variability is consistent with the equilibrium hypothesis, and reflects a lack of 'weather' on air-sea exchange.

b. *Representation of the extreme events*

To further examine the time variability, we compare several time series of temperature taken in the middle of the domain (298°W, 39°N). In Fig. 3a, we compare a 3 months time series of temperature from the ERA reanalysis (thick black line), CheapAML (blue line) and S95 (red line). Both S95 and CheapAML are in good agreement with ERA, with correlations of 0.98 and 0.99 respectively. However bias appears especially in the representation of the extremes (cold and warm events). We plot on Fig. 3b the Probability Density Function (PDF) of these three time series using the same plot convention. CheapAML represents correctly both warm and cold events, if slightly overestimating the cold. The global shape of the ERA PDF is well reproduced — especially the bimodality that is observed during this period. The PDF of the S95 simulation is much more peaked at the center of the distribution. These results reflect the S95 equilibrium hypothesis.

The PDF of humidity at the same location and for the same period is plotted on Fig. 3c. Whereas the S95 simulation has a peaked distribution of humidity, CheapAML recreates more accurately the observed distribution.

The sensible and latent heat flux time series at this location are also well captured by both CheapAML and S95 (correlation above 0.98 in each case). We only show on Fig. 4 the PDF of these time series. The thick black line corresponds to heat fluxes computed using surface fields from ERA but applying the COARE3 formulation. The dashed line corresponds to raw heat fluxes extracted from the ERA dataset. The comparison illustrates the differences inherent to state-of-the-art flux algorithms, which are considerable (see also Appendix A). Once again CheapAML yields a better PDF when compared to the COARE3 implementation than does S95.

c. *Impact on the oceanic circulation*

We now extend the simulations to a more realistic ocean experiment. Our intent is to illustrate the impact of the two AML formulation (S95 and CheapAML) on the oceanic structure. We still focus on the region of the separated GS and use the MITgcm (Marshall et al. 1997) with open boundary conditions. The model obtains boundary data from the HYCOM ocean reanalysis dataset (Chassignet et al. 2007). The starting date is January, 1st 2007 and the model is run for one month. The spatial resolution is 1/12 degrees in latitude and 1/10 degrees in longitude. We use 39 vertical levels with a 'fine' resolution of the upper levels (10 m) and low resolution of the lower level (500 m). This resolution resembles the one employed in many modern global OGCMs. The oceanic mixed layer is computed according to the KPP formulation (Large et al. 1994) and the mixed layer depth is estimated from a Richardson number criteria.

We first compute the air-sea exchange using S95 and then using CheapAML. Since the oceanic states quickly differ after several days, it is not useful to compare the mixed layer depth at a specific location. We plot in Fig. 5 the evolution of the mixed layer depth averaged over the entire domain. The S95 integration is plotted with a dashed line, the CheapAML integration is plotted with a thin line and the HYCOM reanalysis is plotted with a thick line. During this month the mixed layer depth increases everywhere in both simulations, as expected. The first 15 days are well reproduced in the CheapAML run whereas the last 15 days are better reproduced in the S95 run. After one month, we observe a notable difference of 50 m in the two runs whereas the HYCOM reanalysis lies in between this two estimates. The only possible reason to explain these two evolutions lies in the differences in the heat and fresh water fluxes. This illustrates the discrepancies of the oceanic state that occur due to uncertainties in forcings.

The spatial average of net heat flux is given in Fig. 5. The associated mean values for this period are: 303 $\mathrm{W\,m^{-2}}$ for CheapAML, 486 $\mathrm{W\,m^{-2}}$ for S95, 357 $\mathrm{W\,m^{-2}}$ for Hycom, and 304 $\mathrm{W\,m^{-2}}$ for OAFlux (Yu and Weller 2007). The favorable comparison between OAFlux and CheapAML partly reflects their common basis in the COAR3 algorithm, but they do use scatterometer winds while we use ERA winds. The small difference between our numbers is consistent with the idea that local feedbacks on fluxes due to wind modifications by the oceanic mesoscale are not a major systematic error.

The overall character of the means is consistent with the mixed layers diagnosed in the three cases. The interpretation of the differences between The CheapAML and S95 with Hycom is unclear since the latter is an assimilative product.

Nevertheless, we can associate the rapid deepening of the mixed layer with the peaks of the net heat flux. S95, which consistently predicts a higher net heat flux, has a more pronounced mixed layer deepening rate. While all the net heat flux curves are well correlated (above 0.9 for all pairs), the magnitude of the storm peaks are very different. For Jan, 1st (same ocean state for all experiments), we note a difference of 300 $\mathrm{W\,m^{2}}$ between OAFlux and Hycom. The maxima in net flux during storms are either reached by Hycom or S95. In contrast, Hycom, OAFlux and CheapAML agree well at the minima (Jan, 7th and Jan, 16th) — with a difference of less than 50 $\mathrm{W\,m^{2}}$ between them.

4. Global experiment

In the previous section, we demonstrated the benefits of using CheapAML in a regional model. We here show how CheapAML can be used for global experiments, where we again use prescribed SSTs. In a configuration corresponding to the ERA setup (1.125 degrees resolution), we constrain the SST to follow the ERA SST field (perfect ocean model experiment). Over the ocean, we let the air temperature and humidity adjust via CheapAML. The model is initiated in January, 2000 and run for thirteen months; we focus on the last month. We do not have a varying land-sea mask and treat sea-ice points as land points. Atmospheric forcing is drawn from ERA. CheapAML is deployed using standard λ values and ERA boundary layer heights.

a. Atmospheric variables

We compare the mean temperature computed in January 2001 with that in ERA (Fig. 6). The bottom panel of Fig. 6 corresponds to the differences between the middle and the top panel. The largest bias is observed in the Northern hemisphere. More generally, when looking at the June-July-August maps, we conclude that the largest bias occurs in the winter hemisphere. We observe a cold bias near the western boundaries whereas the center of the Atlantic and Pacific are subject to a warm bias. In the tropics, we observe a warm bias in the region of strong convection. These errors reflect processes not modeled here but do not exceed 1.5 degrees C.

Figure 7 focuses on the mean humidity field. Again, we note that the patterns in the two upper panels are in accordance. The humidity maximum in the tropics is well reproduced as are the specific patterns in the extra-tropics. The bottom panel is the difference between the simulated and observed humidity. The maximum differences reach ± 1 g/kg (typically O(5-10%) in the tropics as well as in the extra-tropics. The humidity is mainly overestimated in the northern and southern part of the oceanic basins whereas it is mostly underestimated in the tropics.

The regions where the air temperature or humidity fields are not well estimated reveals the zones where the outgoing flux at the top of the boundary layer or the precipitation is not properly described in our model. Other physical phenomena are thus at work in these regions (convection, clouds, vertical motion). Knowing these discrepancies, one could structure λ so as to minimize model bias.

The precipitation field for January 2001 is plotted on Fig. 8. Although the parameterization mentioned in Sec. 2 is extremely simple, some skill is observed. The two upper panels of Fig. 8 argue that the global patterns of the convective precipitation are well reproduced in the tropics. However, the large scale precipitation in the northern Pacific and Atlantic are underestimated. These precipitations are associated with the position and strength of the stormtrack and can not be easily reproduced using our single layer model.

b. Net heat flux

Figure 9 compares the net heat flux computed by CheapAML with that given by OAFlux (Yu and Weller 2007) for January 2001. CheapAML captures correctly the large scale pattern (enhanced heat flux over the western boundary current in January and North-South asymmetry), but appears to underestimate the heat flux. In the northern hemisphere where the mean heat flux is positive, it is underestimated by $[20 - 70]$ $\mathrm{W\dot{m}^{-2}}$. This pattern is clearly related to the temperature pattern anomaly observed in Fig. 6: an atmosphere that is too warm prevents strong air sea-flux in that region. The difference seen in the southern hemisphere has a pattern that is very similar to the humidity differences: a dry mixed layer leads to a larger evaporation and thus an increase of the net heat flux. In July the situation is reversed (not shown). This is also in accordance with the temperature and humidity differences observed in July (not shown): the northern hemisphere Qnet is large enough. Note also that some differences might also be explained by the longwave parameterization (see Eq. 8), although this heat source remains small compared to the sensible and latent heat flux.

5. Conclusions

a. Summary

We introduce here a simple atmospheric boundary layer model for the computation of air-sea exchange in ocean-only modeling. In the boundary layer, temperature and humidity are advected by a prescribed wind. Temperature and humidity adjust with the underlying SST mainly through sensible and latent heat exchanges. The value of this model is to capture part of the non-local feedback of the ocean surface on air-sea exchanges, while stopping well short of computing a full coupled ocean-atmosphere model. We believe that for an oceanic model, it is preferable to use CheapAML than to prescribe the temperature and humidity (or fluxes) from a reanalysis data set: as soon as the oceanic state deviates from the observed state, the reanalysis temperature and humidity fields and the oceanic state are not related anymore. The computational cost of using CheapAML is minimal, and does not materially increase the execution time of the model run. Furthermore, CheapAML captures the 'weather' impacts of the atmosphere on air-sea exchange with improved fidelity relative to its predecessor, S95.

Using a regional and a global configuration we tested the skills of CheapAML. In a small region subject to large spatial variations of SST, we show that this slab atmospheric model is able to accurately reconstruct the mean temperature and humidity fields as well as their variability. Analyzing several time series of atmospheric tracers and fluxes at given locations, we argue that CheapAML reproduces the mean as well as the extreme events correctly. The extreme events (for e.g. cold air outbreak) are of great importance for the oceanic dynamics. We illustrate this impact using the evolution of the mixed layer depth when the ocean is subject to these different fluxes. When deployed globally, zones appear where temperature and humidity are subject to biases. These biases, although small, are inherent to the simplifications performed to construct this model, and can be reduced through nudging.

The main differences between this model and its predecessor Seager et al. (1995) are the elimination of the equilibrium assumption and the provision of a water budget. Here, we explicitly integrate in time the equation of evolution of temperature and humidity. We also updated the computation of the air-sea fluxes using a more recent formulation (Fairall et al. 2003). An accurate computation of the air-sea fluxes is in fact the primary goal of this study. The fresh water flux budget exhibits similarity with the observed fresh water budget although a better representation of precipitation might help to increase the accuracy of this forcing. Moreover, we propose here a fully parallel code whereas the computation of S95 requires the knowledge of atmospheric variables in the entire domain and is thus harder to parallelize.

b. *Remaining issues*

Among issues for future development are the development of atmosphere-land and atmosphere sea-ice modules. Such regions are handled by means of strong relaxation towards specified values; these are clear areas for improvement.

Clouds are also not parameterized in this model. It is however possible to adjust the solar input to mimic the presence of clouds, although not dynamically.

Several studies (see Small et al. 2008, for a review) indicate that there is a small correlation observed between the wind speed and the SST; the wind being accelerated over warm SST. This interaction could also lead to some possible refinement of our model, especially in regions of strong SST fronts or eddies. Pezzi et al. (2004) and Jin et al. (2009) proposed parameterizations of the wind–mesoscale eddies interaction. According to their results, the detailed structure of the oceanic eddies is affected by this interaction. How this may impact the large scale ocean circulation remains to be seen.

c. Practical use of CheapAML

We recommend the use of CheapAML via the MITgcm (Marshall et al. 1997), where it was first developed as a package. Several options are available, e.g. formulation of the fluxes (LP82 or COARE 3) or choice of the advection scheme (flux limited versus centered differences). It can be used either for regional modeling purposes (open boundary conditions) or for global modeling (zonally periodic boundary conditions). The current version of CheapAML assumes the model domain is bounded by constant grid lines, eg, for a sphere, the boundary consists of one northern and one southern latitude, and single eastern and western longitudes.

Acknowledgments.

We thank Jean-Michel Campin and Chris Hill for their valuable help. The final version has benefited from detailed comments by Richard Seager and one anonymous reviewer. This work was supported by NSF grant number OCE-0960500.

APPENDIX

The turbulent air-sea fluxes

Figure 10 is an example of the differences observed in the strength of the latent and sensible heat fluxes when computed using several methods. Several studies already mention the differences between these products (cf. Kubota et al. (2008) and references therein for an example over the Kuroshio Extension or Rouault et al. (2003) for the aghulas current or Kubota et al. (2003) for a global comparison).

We report four different computations of the turbulent heat fluxes for January 2007: the ERA reanalysis Beljaars (1994), the NCEP/NCAR reanalysis Kalnay et al. (1996), COARE 3 using ERA temperature, humidity and wind and LP82 also using ERA surface variables.

We observe large differences especially for the sensible heat flux estimations. The latent and sensible heat fluxes are maximum when estimated with LP82. They reach respectively 670 and 250°W m^{-2}. The patterns are the same for three computation that uses ERA reanalysis. It reflects the presence of meanders in the GS. The coarse resolution of the NCEP/NCAR reanalysis does not allow a fine comparison. However we clearly see that there is a good agreement in the magnitude of NCEP and COARE 3.

The comparison of SH-ERA40 and SH-COARE3 is consistent with Fig. 4. It appears that ERA40 produces significantly lower sensible heat fluxes than COARE3. This difference of almost 100 W m^2 over the warm core of the Gulf Stream can have tremendous effects on the oceanic circulation as illustrated in Fig. 5. Since all atmospheric and oceanic variables are the same in that case in this computation, this difference is only due to the estimation of the exchange coefficient C_d (see Eq. 14).

REFERENCES

Beljaars, A. C. M., 1994: The parametrization of surface fluxes in large-scale models under free convection. *Quart. J. Roy. Meteor. Soc.*, **121**, 255–270, doi:10.1002/qj.49712152203.

Chassignet, E. P., H. E. Hurlburt, O. M. Smedstad, G. R. Halliwell, P. J. Hogan, A. J. Wallcraft, R. Baraille, and R. Bleck, 2007: The HYCOM (HYbrid Coordinate Ocean Model) data assimilative system. *J. Mar. Syst.*, **65**, 60–83, doi:10.1016/j.jmarsys.2005.09.016.

Clark, N. E., L. Eber, R. M. Laurs, J. A. Renner, and J. F. T. Saur, 1974: Heat exchange between ocean and atmosphere in the eastern north pacific for 1961-71. Tech. Rep. NMFS SSRF-682, NOAA.

Fairall, C. W., E. F. Bradley, J. E. Hare, A. A. Grachev, and J. B. Edson, 2003: Bulk parameterization of air sea fluxes: Updates and verification for the COARE algorithm. *J. Climate*, **16**, 571–591, doi:10.1175/1520-0442(2003)016⟨0571:BPOASF⟩2.0.CO;2.

Hazeleger, W., R. Seager, M. Visbeck, N. Naik, and K. Rodgers, 2001: Impact of the midlatitude storm track on the upper pacific ocean. *J. Phys. Oceanogr.*, **31**, 616–636, doi:10.1175/1520-0485(2001)031⟨0616:IOTMST⟩2.0.CO;2.

Jin, X., C. Dong, J. Kurian, J. C. McWilliams, D. B. Chelton, and Z. Li, 2009: SST-Wind interaction in coastal upwelling: Oceanic simulation with empirical coupling. *J. Phys. Oceanogr.*, **39**, 2957–2970, doi:10.1175/2009JPO4205.1.

Josey, S. A., D. Oakley, and R. W. Pascal, 1997: On estimating the atmospheric longwave flux at the ocean surface from ship meteorological reports. *J. Geophys. Res.*, **102**, 27 961–27 972, doi:10.1029/97JC02420.

Kalnay, E. et al., 1996: The NCEP/NCAR 40-year reanalysis project. *Bull. Amer. Meteorol. Soc.*, **77**, 437–472, doi:10.1175/1520-0477(1996)077⟨0437:TNYRP⟩2.0.CO;2.

Kubota, M., N. Iwabe, M. F. Cronin, and H. Tomita, 2008: Surface heat fluxes from the NCEP/NCAR and NCEP/DOE reanalyses at the kuroshio extension observatory buoy site. *J. Geophys. Res.*, **113 (C12)**, C02 009, doi:10.1029/2007JC004338.

Kubota, M., A. Kano, H. Muramatsu, and H. Tomita, 2003: Intercomparison of various surface latent heat flux fields. *J. Climate*, **16**, 670–678, doi:10.1175/1520-0442(2003)016⟨0670:IOVSLH⟩2.0.CO;2.

Large, W. G., J. C. McWilliams, and S. C. Doney, 1994: Oceanic vertical mixing: a review and a model with a nonlocal boundary layer parameterization. *Rev. Geophys.*, **32**, 363–404, doi:10.1029/94RG01872.

Large, W. G. and S. Pond, 1982: Sensible and latent heat flux measurements over the ocean. *J. Phys. Oceanogr.*, **12**, 464–482, doi:10.1175/1520-0485(1982)012⟨0464:SALHFM⟩2.0.CO;2.

Marshall, J., A. Adcroft, C. Hill, L. Perelman, and C. Heisey, 1997: A finite-volume, incompressible Navier Stokes model for studies of the ocean on parallel computers. *J. Geophys. Res.*, **102**, 5753–5766, doi:10.1029/96JC02775.

Pezzi, L. P., J. Vialard, K. J. Richards, C. Menkes, and D. Anderson, 2004: Influence of ocean-atmosphere coupling on the properties of tropical instability waves. *Geophys. Res. Lett.*, **31**, L16306, doi:10.1029/2004GL019995.

Rouault, M., C. J. C. Reason, J. R. E. Lutjeharms, and A. C. M. Beljaars, 2003: Underestimation of latent and sensible heat fluxes above the agulhas current in NCEP and ECMWF analyses. *J. Climate*, **16**, 776–782, doi:10.1175/1520-0442(2003)016⟨0776:UOLASH⟩2.0.CO;2.

Seager, R., M. Blumenthal, and Y. Kushnir, 1995: An advective atmospheric mixed layer model for ocean modeling purposes: Global simulation of surface heat fluxes. *J. Climate*, **8**, 1951–1964, doi:10.1175/1520-0442(1995)008⟨1951:AAAMLM⟩2.0.CO;2.

Small, R. J., et al., 2008: Air-sea interaction over ocean fronts and eddies. *Dyn. Atmos. Ocean*, **45**, 274–319.

Smith, S. D., 1988: Coefficients for sea surface wind stress, heat flux, and wind profiles as a function of wind speed and temperature. *J. Geophys. Res.*, **93**, 15 467–15 472, doi:10.1029/JC093iC12p15467.

Talley, L., G. Pickard, W. Emery, and J. Swift, 2011: *Descriptive Physical Oceanography: An Introduction*. Academic Press, Elsevier Science.

Uppala, S. M. et al., 2005: The ERA-40 re-analysis. *Quart. J. Roy. Meteor. Soc.*, **131**, 2961–3012, doi:10.1256/qj.04.176.

Yu, L. and R. A. Weller, 2007: Objectively analyzed air sea heat fluxes for the global ice-free oceans (1981 2005). *Bull. Amer. Meteorol. Soc.*, **88**, 527, doi:10.1175/BAMS-88-4-527.

List of Figures

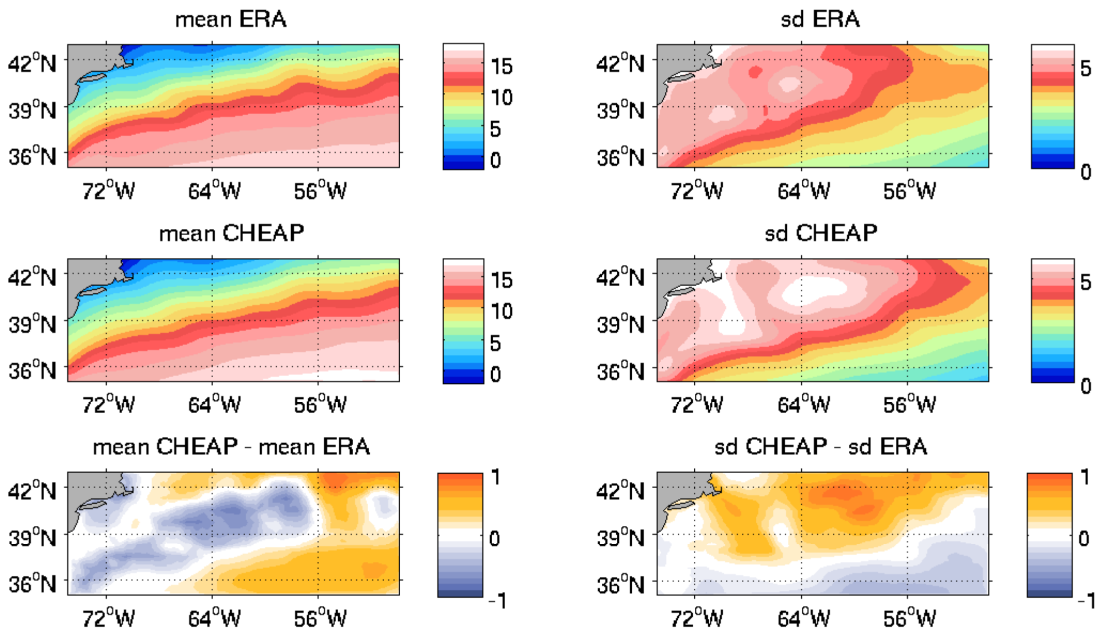

FIG. 1. Upper panels: mean lower layer atmospheric temperature (left) and standard deviation of daily values from that mean (right) in January 2007 (daily data from ERA). Middle panels: same fields but reconstructed with a one month CheapAML integration (starting date: January, 1st 2007). Lower panels: difference between the middle and upper panel. (units are degrees Celsius)

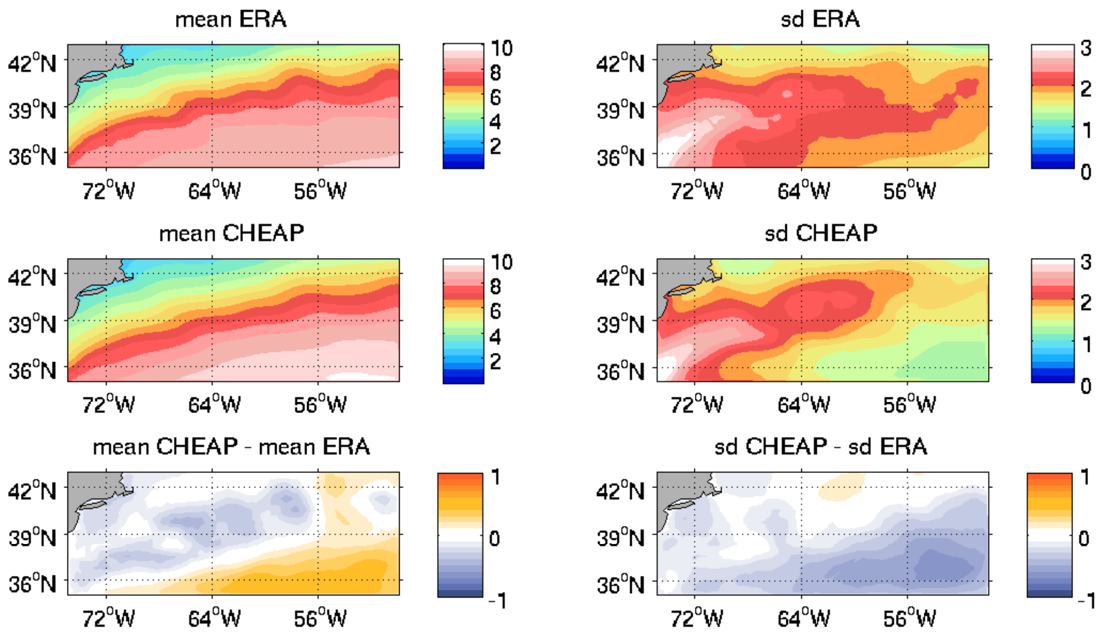

FIG. 2. Same as Fig. 1 but for humidity. (units are g/kg)

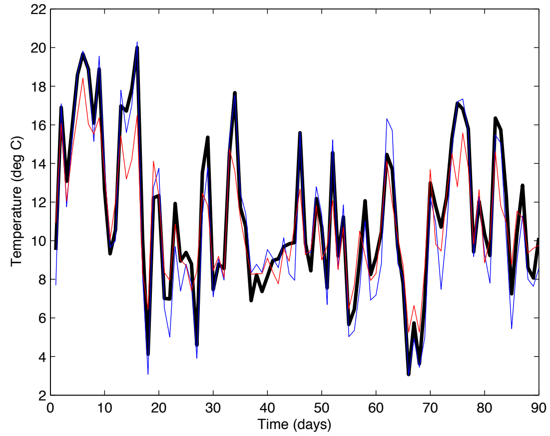

(a)

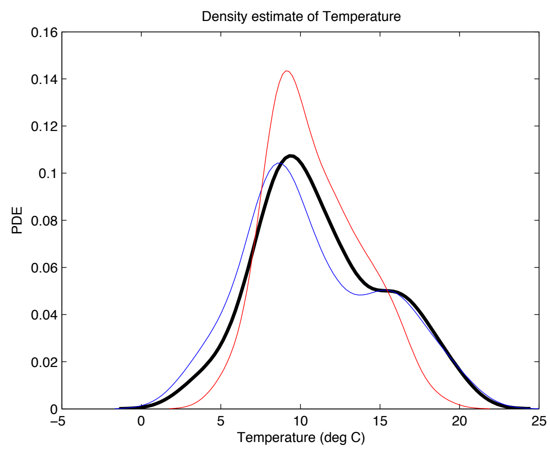

(b)

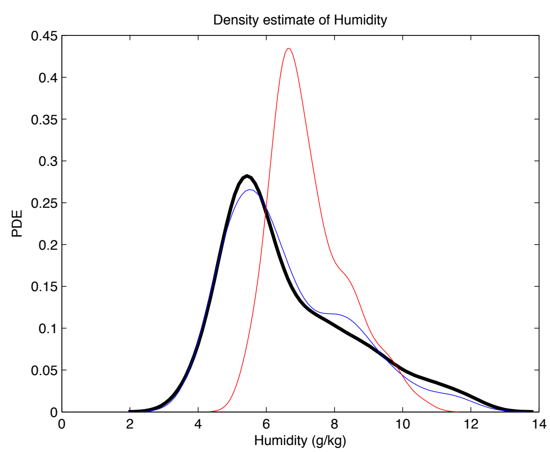

(c)

FIG. 3. Top: time series of the atmospheric temperature in the middle of the regional model (cf. Figs. 1-2) from January, 1st 2007 to Mar, 31st 2007. The thick black line is the ERA temperature; blue CheapAML and red is S95. Middle: PDF of these three time series. Bottom: PDF of the humidity time series using the same color conventions.

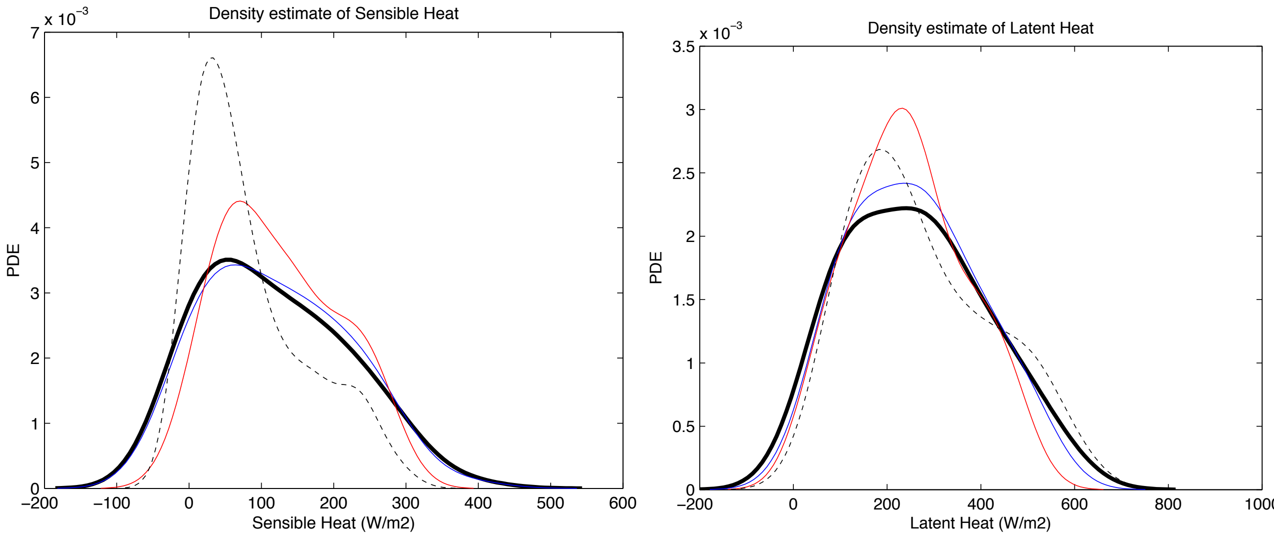

(a) (b)

FIG. 4. PDF of the latent and sensible heat fluxes for the first three month of 2007. Thick black line corresponds to the fluxes computed using the ERA fields with the COARE3 algorithm, the dashed line is the raw ERA fluxes, the blue line is the fluxes using CheapAML and the red line represents S95.

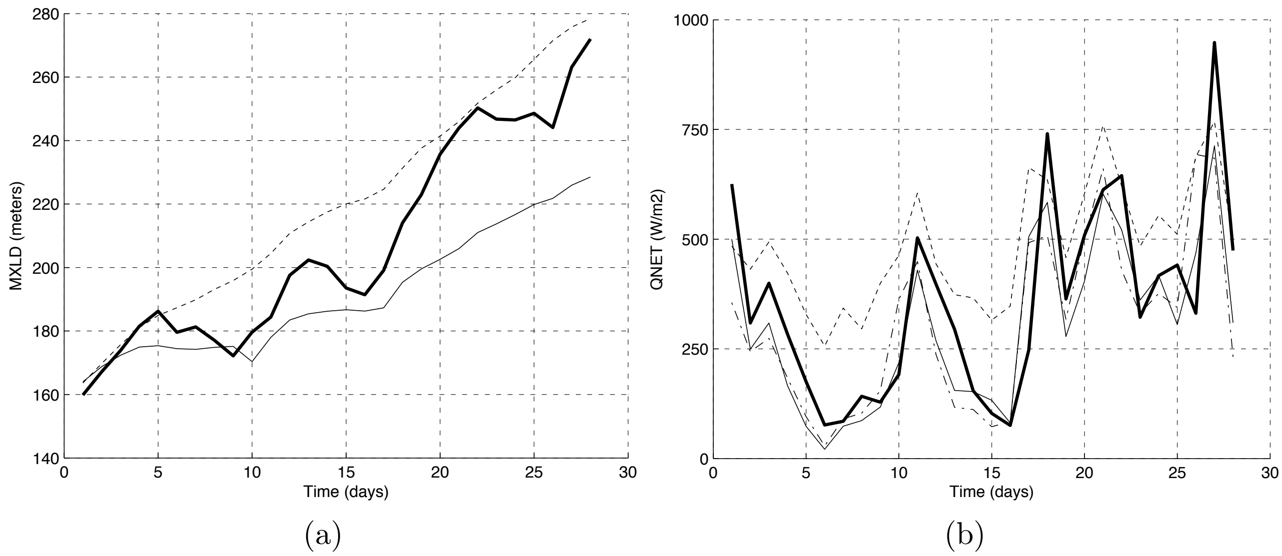

FIG. 5. Left: 30 days time series of the mean mixed layer depth for three oceanic states: Hycom reanalysis (thick line), CheapAML run (thin line) and S95 run (dashed line). Right: corresponding net heat flux averaged over the domain. The additional curve (dashed-dotted) corresponds to the OA flux value.

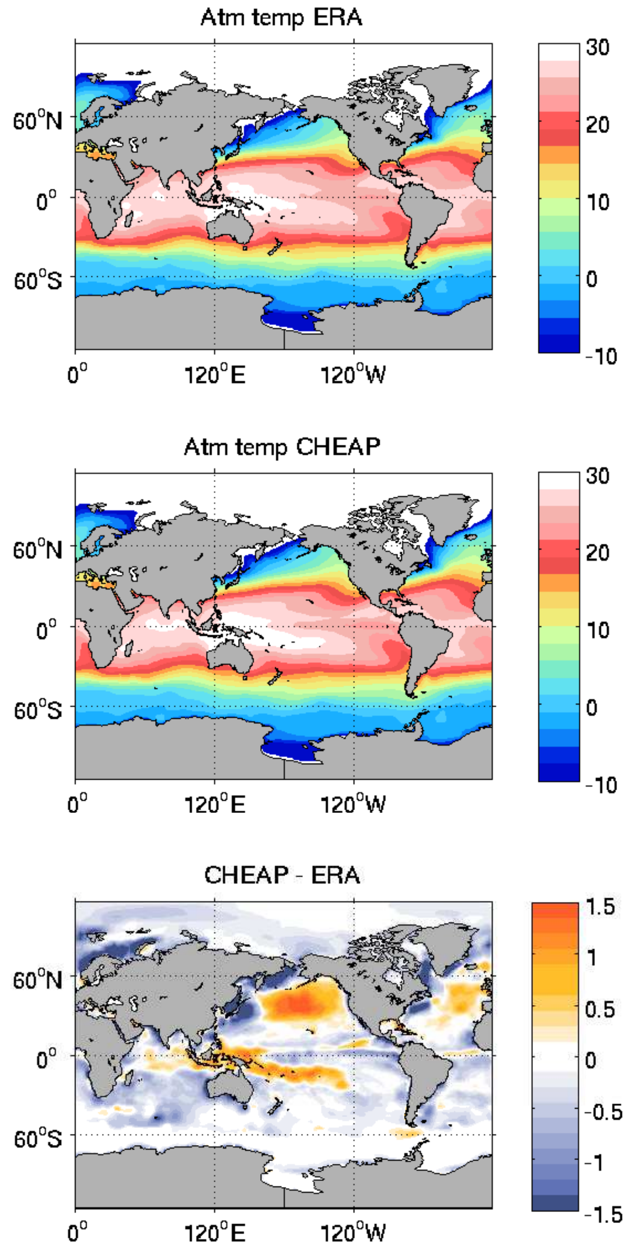

FIG. 6. Top: mean atmospheric lower layer temperature in January 2001 (data from ERA). Middle: reconstructed temperature in January 2001 with CheapAML starting in January 1st 2000. Lower panel: difference between the middle and top panel. (units are degrees C)

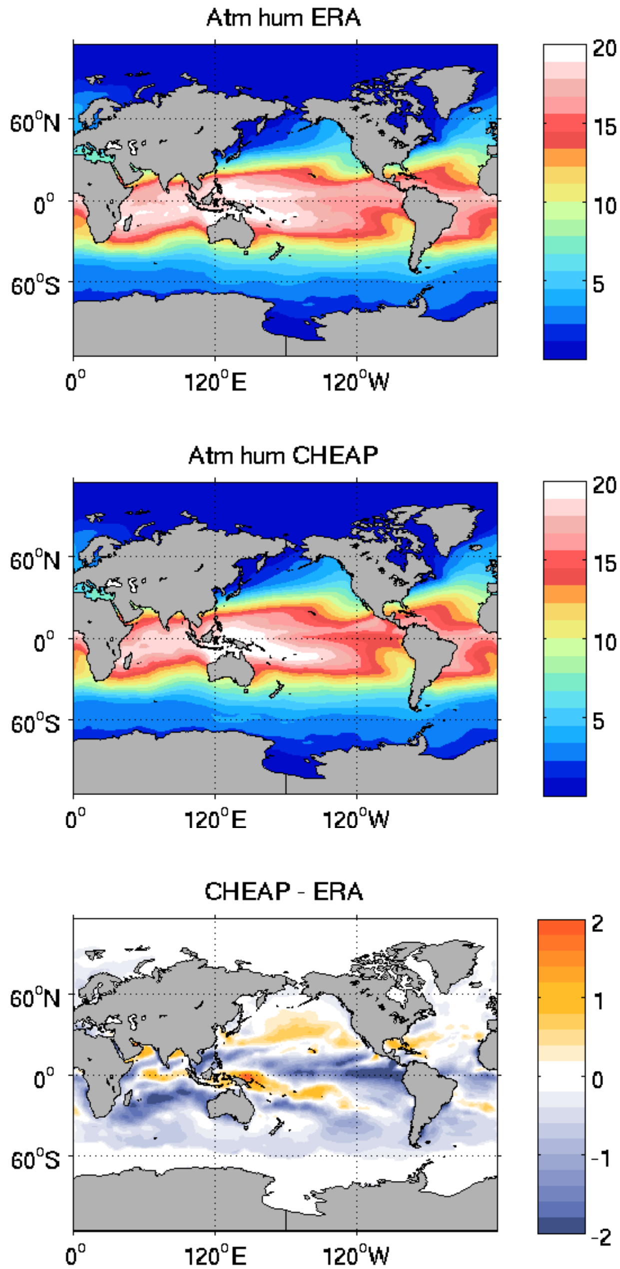

Fig. 7. Same as Fig. 6 but for humidity (units are g/kg).

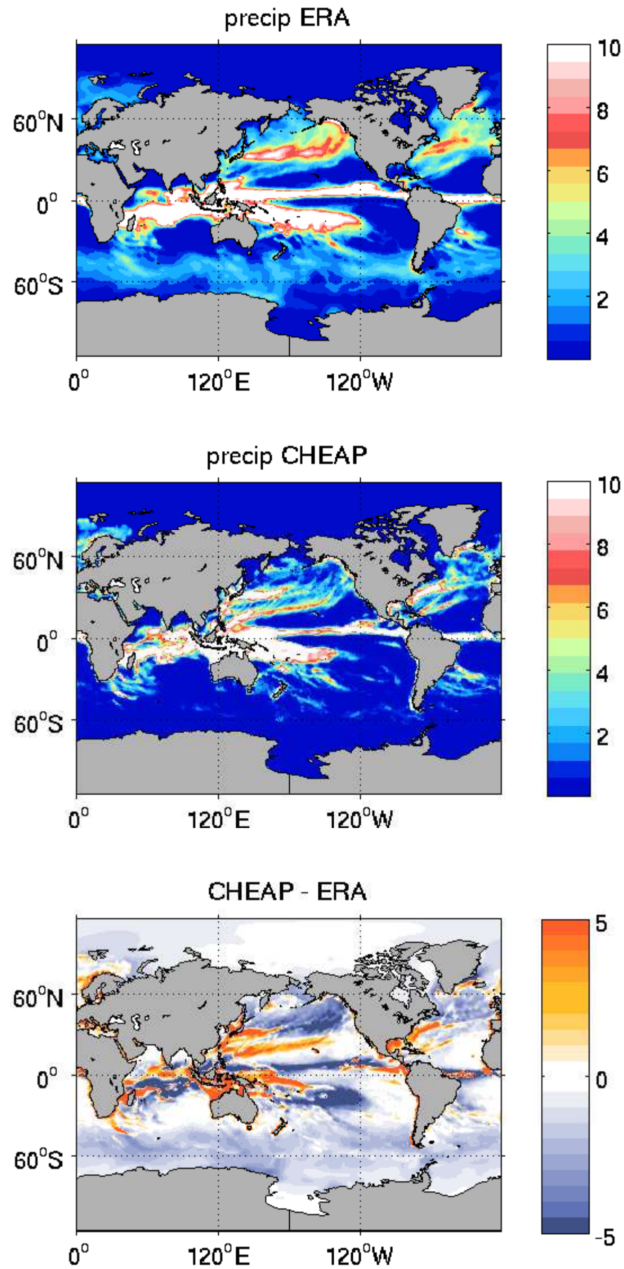

FIG. 8. Same as Fig. 6 but for precipitation (units: mm/day).

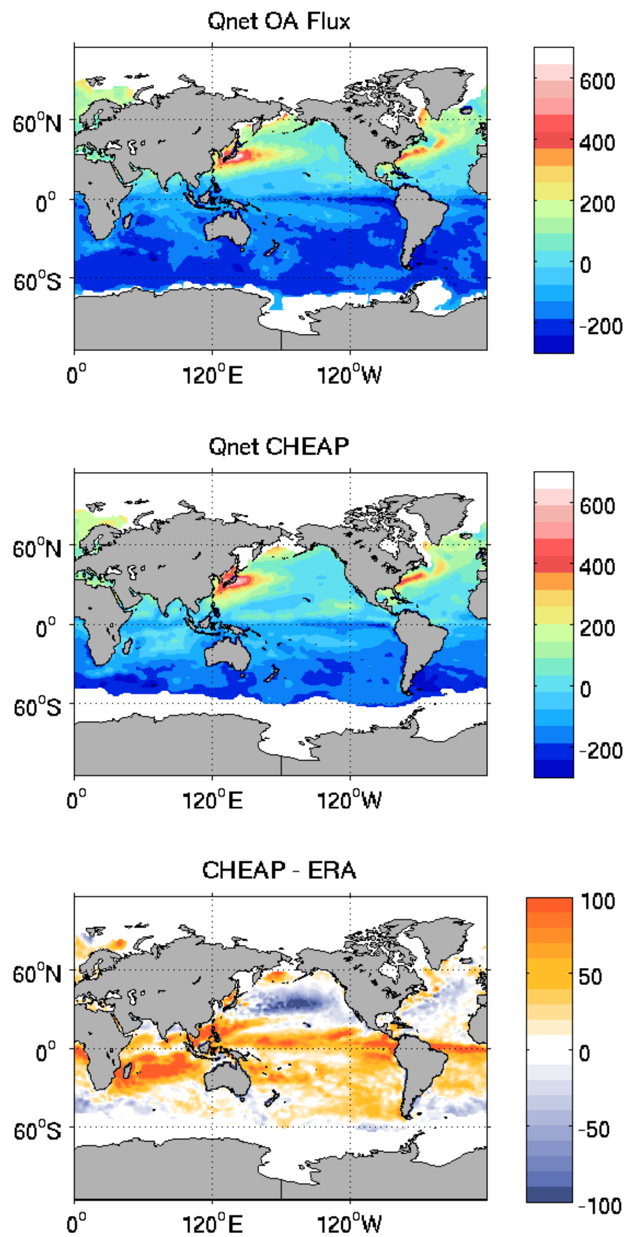

FIG. 9. Same as Fig. 6 but for Qnet (units: W$\dot{m}^{-2}$).

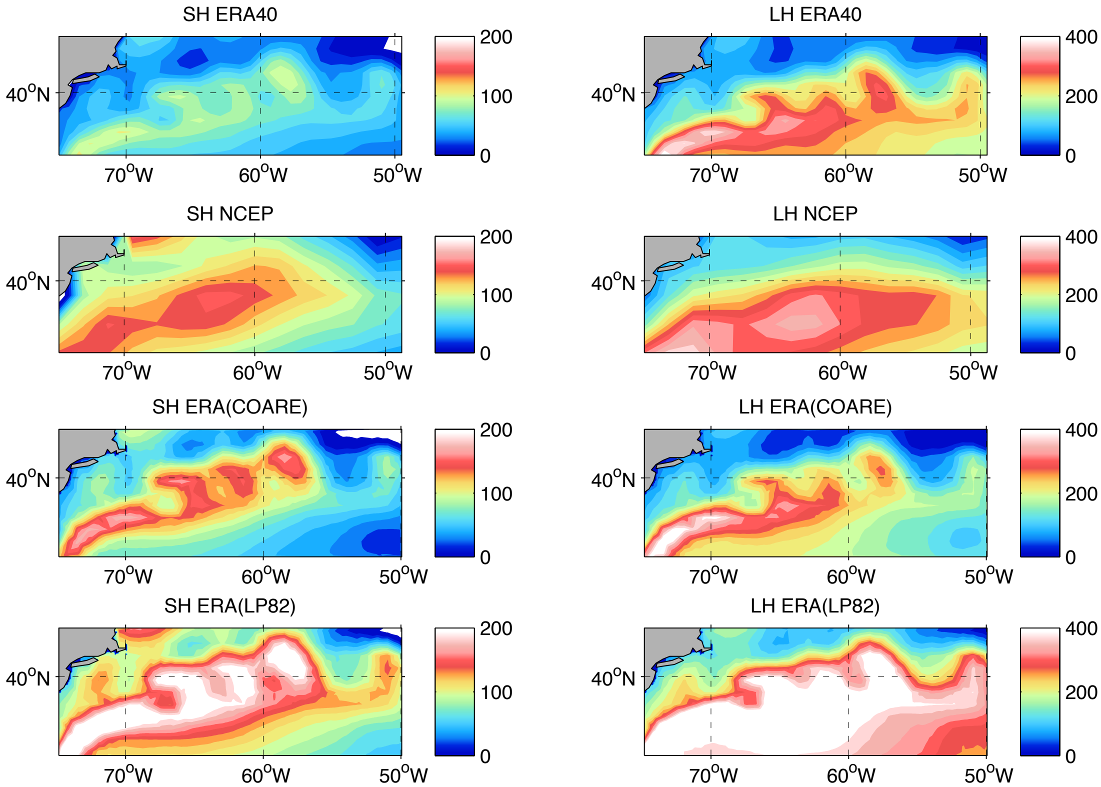

FIG. 10. Comparison of sensible (left column) and latent (right column) heat fluxes computed using different bulk formulae in January 2007. First row: ERA values Beljaars (1994); second row NCEP/NCAR reanalysis; third row: COARE 3 using ERA atmospheric and oceanic fields; last row: LP82 using ERA atmospheric and oceanic fields. (units are $\mathrm{W\,m^{-2}}$)